

# Wave turbulence in driven dipolar gases

G. Bougas,<sup>1</sup> K. Mukherjee,<sup>2</sup> and S. I. Mistakidis<sup>1</sup>

<sup>1</sup>*Department of Physics, Missouri University of Science and Technology, Rolla, MO 65409, USA*

<sup>2</sup>*Mathematical Physics and NanoLund, LTH, Lund University, Box 118, 22100 Lund, Sweden*

(Dated: October 21, 2024)

The nonequilibrium turbulent response of driven three-dimensional dipolar gases is monitored by dynamically crossing the supersolid-to-superfluid phase transition and vice versa utilizing a periodically modulated scattering length. Following the generation of vortical defects in the bulk, a direct cascade front emerges transporting energy from larger to smaller length scales and leading to a nonequilibrium quasi-steady state at long evolution times. This quasi-steady state is evidenced by the self-similar character of the momentum distributions featuring an algebraic reduction at large momenta with scaling exponents supporting the existence of wave turbulence. We observe that supersolidity sustaining higher-lying momenta, associated with the roton minimum, promotes the emergence of turbulence. Our results provide a stepping stone for unravelling and exploiting turbulent and self-similar behavior in anisotropically interacting quantum gases amenable in current experiments.

*Introduction.* Turbulence is a ubiquitous hydrodynamic phenomenon associated with direct (inverse) energy cascades from larger (smaller) to smaller (larger) length scales [1]. It has an unambiguously interdisciplinary role determining the flow of fluids [2], the formation of polymers [3], the climate of planets [4], as well as star explosions [5]. Due to the many degrees of freedom involved, providing a microscopic description of turbulence is challenging. Instead, statistical models are capable to capture the energy transfer, mediated either through vortices or nonlinear waves, alias vortex and wave turbulence respectively [6–8].

These complex transfer processes can be monitored in a controllable fashion in the realm of ultracold quantum gases [9, 10]. These platforms provide leverage on turbulence, allowing to track vortex reconnections and annihilations [11, 12], as well as the propagation of cascade fronts [13] and eventually the emergence of nonequilibrium steady states [14]. Strikingly, initiation of inverse cascades in superfluids (SF) [15], and the formation of stratified turbulence by tuning the polarizability of dipolar cold atoms [16] have been demonstrated.

Long-range interacting gases [17], such as dipolar settings hosting exotic phases of matter, provide fertile platforms to control turbulent flow [18, 19], as was already evinced in their classical counterparts, the ferrofluids [20]. These magnetic atomic systems commonly consisting of lanthanides [21–23] sustain self-bound droplet arrays [24–26], which can be even connected by a SF background forming supersolids (SS) [27, 28]. Such states were observed in both elongated [29–32] and planar geometries [33–35]. They originate from the softening of a roton minimum, modifying the momentum distribution with respect to that of a SF [36, 37], which can be utilized to engineer the onset and characteristics of turbulence. In fact, the impact of such exotic phases of matter, featuring shear modulus and frictionless mass transport, see [38, 39] and references therein, on the turbulent re-

sponse remains elusive. Moreover, since they require the presence of quantum fluctuations [40, 41] for their stabilization, they share the premise to bring forth beyond mean-field aspects of turbulence as well.

In this Letter, we showcase the progressive emergence of quantum turbulence in the nonequilibrium dynamics of anisotropically long-range interacting circularly-shaped dipolar Bose-Einstein condensates (BECs) with the first-order quantum correction term. The magnetic atoms are prepared in one of the SS or SF phases and a periodic driving of the 3D scattering length is deployed to dynamically cross the ensuing phase boundaries known from the ground state [42]. The turbulent response is captured by the self-similar long-time behavior of the momentum distribution (or mode occupation number) at large wavenumbers, which exhibits an algebraic reduction with averaged scaling exponents over all driving frequencies  $\gamma \approx 3.25$  and  $\beta \approx 0.8$ , alluding to wave turbulence [9, 13]. The dynamics is characterized by a direct energy cascade front which becomes gradually statistically isotropic at the nonequilibrium quasi-steady state. The latter occurs irrespective of the initial state and the driving frequency when dynamically crossing the phase transitions. Interestingly, non-conventional initial SS and droplet states accelerate the manifestation of turbulence due to their extended momentum distribution.

*Dipolar gas and driving protocol.* We consider a dipolar gas of  $8 \times 10^4$   $^{164}\text{Dy}$  atoms of mass  $m$  polarized along the  $z$ -axis and confined in a cylindrically symmetric harmonic trap  $V(\mathbf{r})$  with frequencies  $(\omega_x, \omega_y, \omega_z) = 2\pi \times (43, 43, 133)$  Hz as in the experiments of Refs. [43, 44]. At zero temperatures and within the weakly interacting regime [17], the dynamics of the dipolar gas can be adequately captured within the extended Gross-Pitaevskii framework [45, 46],

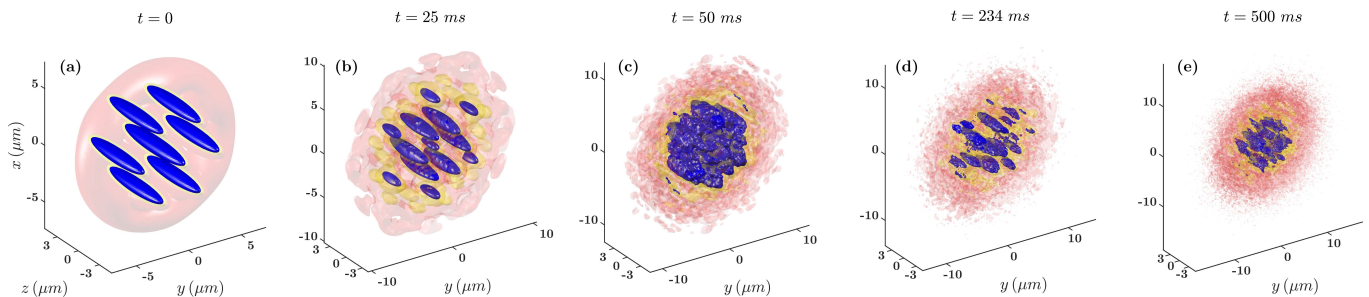


FIG. 1. Emergence of wave turbulence at long evolution times [panels (c)-(e)] of a periodically driven dipolar SS [panel (a)] across the SS-to-SF phase transition. Three dimensional density isosurfaces [referring to 1% (red), 10% (yellow) and 25% (blue) of the 3D peak densities] at different time instants of the evolution. The initial (final) 3D scattering length is  $a_i = 89 a_0$  ( $a_f = 98 a_0$ ) and the driving frequency  $\omega_d = 2\pi \times 127$  Hz.

$$i\hbar\partial_t\Psi(\mathbf{r}, t) = \left[ -\frac{\hbar^2}{2m}\nabla^2 + V(\mathbf{r}) + \frac{4\pi\hbar^2 a}{m} |\Psi(\mathbf{r}, t)|^2 + \int d\mathbf{r}' U_{dd}(\mathbf{r} - \mathbf{r}') |\Psi(\mathbf{r}', t)|^2 + \gamma(\epsilon_{dd}) |\Psi(\mathbf{r}, t)|^3 \right] \Psi(\mathbf{r}, t). \quad (1)$$

The 3D scattering length,  $a$ , can be experimentally tuned via Fano-Feshbach resonances [47, 48]. The dipolar interaction  $U_{dd}(\mathbf{r}) = \frac{3\hbar^2 a_{dd}}{m} \left[ \frac{1-3\cos^2\theta}{r^3} \right]$  contains the angle  $\theta$  between the relative distance  $\mathbf{r} = (x, y, z)$  of two dipoles and the  $z$  quantization axis, while  $a_{dd} = 131 a_0$  is the  $^{164}\text{Dy}$  dipolar length with  $a_0$  denoting the Bohr radius. The fifth term is the repulsive first-order beyond mean-field Lee-Huang-Yang energy correction within the local density approximation, where  $\gamma(\epsilon_{dd}) = \frac{128\pi\hbar^2 a}{3m} \sqrt{a^3/\pi} (1 + \frac{3}{2}\epsilon_{dd}^2)$ , and  $\epsilon_{dd} \equiv a_{dd}/a$  [49, 50]. The interplay between short-range (third term) and long-range (fourth term) interactions in the presence of quantum fluctuations yields a rich phase diagram [17]. It features the SF phase at  $a/a_0 > 93$ , as well as high-density exotic states being the SS for  $87 \leq a/a_0 \leq 93$ , and the droplet arrays at  $a/a_0 \leq 86$  in our considered setup.

The dipolar gas is initialized in one of the above phases characterized by a specific initial scattering length  $a_i$ , see supplemental material (SM) [51] for more details on the initialization and the numerical method. Capitalizing on the tunability of the scattering length, the latter is subsequently periodically modulated with frequency  $\omega_d$  according to  $a(t) = a_i + (a_f - a_i) \sin^2(\omega_d t)$ , where  $\omega_d \gtrsim \omega_x$ . Sufficiently large modulation amplitudes ( $a_f - a_i$ ) trigger the dynamical crossing between different phases, arising at the ground state level at scattering lengths  $a_i$  and  $a_f$ .

*Density profiles and direct energy cascade.* We initialize the dipolar condensate at  $a_i = 89 a_0$ , where a SS state emerges. In quasi-2D geometries, such a state is typically characterized by spontaneously formed density peaks (droplets) arranged in a hexagonal structure on

top of a SF background [Fig. 1(a)] [42, 44].

Setting  $a_f = 98 a_0$ , which represents a SF state at the ground state level, the dipolar gas is consecutively periodically driven across the SS-to-SF phase transition. During the early stages of the evolution the initial hexagonal crystal symmetry is gradually broken, as evidenced by the densities depicted in Fig. 1(b),(c). Instead, high density peaks start to distribute randomly and the SF background becomes substantially perturbed. In the process, a collective motion of the entire gas occurs, while a small number of defects in the form of vortex dipoles builds upon the SF background which annihilate or drift out of the condensate. The aforementioned density perturbation proliferates in the course of the evolution [Fig. 1(d),(e)], rendering the background distribution similar to that of a non-dipolar SF experiencing wave turbulence [13, 52].

The turbulent stage appears to be independent of the driving frequency, in contrast to the dynamical response at early evolution times which strongly depends on both the driving characteristics and the initial state. To ascertain whether turbulence develops during the long time dynamics, we examine the momentum distribution in the transverse plane defined as  $n(\mathbf{k}, t) = \left| \int d\mathbf{r}_{\parallel} e^{-i\mathbf{k}\cdot\mathbf{r}_{\parallel}} \sqrt{\int dz |\Psi(\mathbf{r}_{\parallel}, z, t)|^2} \right|^2$ , where  $\mathbf{k} = (k_x, k_y)$  and  $\mathbf{r}_{\parallel} = (x, y)$ . Probing this distribution, which can be experimentally monitored via Bragg spectroscopy [13], is motivated by the practically frozen dynamics along the  $z$  direction compared to the planar motion [see also Fig. 1]. Strikingly, for  $t > 200$  ms this distribution becomes nearly isotropic in the  $x$ - $y$  plane at large  $|\mathbf{k}|$  [13] despite the presence of anisotropic interactions [see Eq. (1)], as evidenced by the ratio of integrated densities  $n_x/n_y = \frac{\int dk_y n(\mathbf{k}, t)}{\int dk_x n(\mathbf{k}, t)}$  in the inset of Fig. 2(a). Therefore the azimuthal average  $\bar{n}(|\mathbf{k}|, t) = \int d\phi n(|\mathbf{k}|, \phi, t)$  is a more suitable measure for demonstrating turbulence properties [11].

The momentum distribution displays a power-law behavior at large momenta  $|\mathbf{k}| \gg |\mathbf{k}_{\text{rot}}|$ , where  $|\mathbf{k}_{\text{rot}}| l_s \simeq$

0.177 is the roton minimum. Here,  $l_s = \hbar/\sqrt{m\mu}$  is the length scale determined by the chemical potential  $\mu$  of the initial state. By fitting the  $\tilde{n}(|\mathbf{k}|, t)$  distribution with  $|\mathbf{k}|^{-\gamma}$  in the region  $|\mathbf{k}| \in [0.6, 1.1] l_s^{-1}$  at  $t = 800$  ms we extract the exponent  $\gamma = 2.8$ , alluding to wave turbulence [8], which originates from nonlinear wave mixing [9]. Recall that in the case of weak interactions where the generated waves possess random phases, the so-called weak wave turbulence regime is entered characterized by  $\gamma \simeq 3$  [7, 52, 53]. The discrepancy between our exponent and this value may be partially due to the appearance of the small number of defects as also argued in the case of a non-dipolar SF undergoing wave turbulence [9], higher order corrections to the cascade scaling [52], or long-range interactions. It is also interesting to note that a similar power-law behavior and exponent appear in the presence of three-body losses, where a more drastic descent of  $\tilde{n}(|\mathbf{k}|, t)$  occurs, in line with experimental observations [13], see SM for details [51]). We also remark that the above-described turbulent response characterized by the exponent  $\gamma \sim 3$  holds for the non-viscous SS considered herein. However, the inclusion of viscosity through a phenomenological damping term diminishes long-wavelength excitations enforcing a rapid reduction of high-momentum tails and leading to larger values of  $\gamma$ , see also SM [51].

The momentum distribution compensated with  $|\mathbf{k}|^\gamma$ , evolves towards a plateau around  $l_s^{-1}$  [Fig. 2(a)], demonstrating the development of a nonequilibrium quasi-steady state [9, 14, 53]. Before reaching that state, the slope of the compensated distribution's tail continuously decreases, marking the progression of a cascade front [13] towards higher momenta. This is a clean manifestation of a direct energy cascade [53]. The fitted exponent at these early times continuously decreases before eventually approaching  $\gamma \approx 2.8$ . Moreover, the 2D kinetic energy density  $\mathcal{E}(|\mathbf{k}|, t)$  displays a power-law behavior around  $|\mathbf{k}|l_s \simeq 1$  as well, and the respective exponent saturates close to  $-1$ , as expected from the scaling relation,  $\mathcal{E}(|\mathbf{k}|, t) = \frac{\hbar^2 |\mathbf{k}|^2}{m} \tilde{n}(|\mathbf{k}|, t)$ .

Notably, wave turbulence consistently arises across a broad range of driving frequencies [9], see for instance the time-evolution of the power-law exponents for  $\omega_d \in [1, 5]\omega_x$  illustrated in Fig. 2(b). At long evolution times where saturation occurs, the mean value of the exponent over the driving frequencies is 3.25, indicated by the dashed line in Fig. 2(b). In fact, the driving frequency slightly affects the saturation value of the exponent, leading to the standard deviation 0.26.

*Impact of the initial state.* We subsequently investigate the role of the initial state on the turbulent response, by dynamically crossing the phase transition inversely, i.e., from a SF ( $a_i = 98 a_0$ ) to a SS ( $a_f = 91 a_0$ ). At  $t \gtrsim 300$  ms, significant density undulations arise which gradually develop into a wave turbulent cascade quanti-

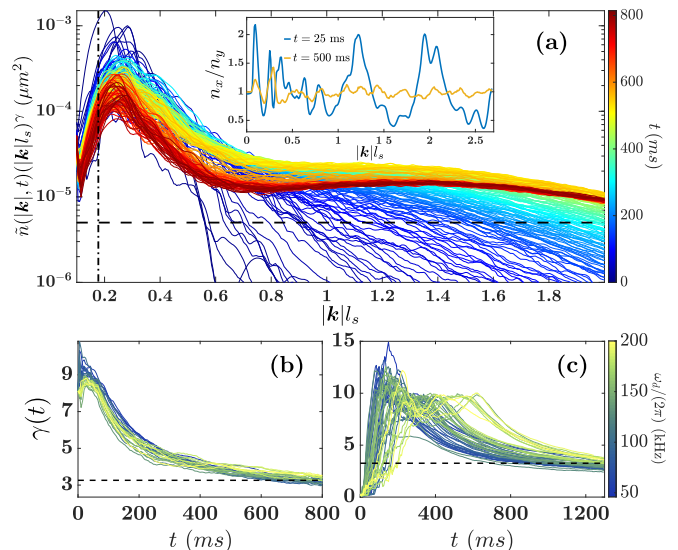


FIG. 2. Quantification of the self-similar turbulent response and its independence on the driving frequency and initial state. (a) Compensated momentum distribution  $\tilde{n}(|\mathbf{k}|, t)(|\mathbf{k}|l_s)^\gamma$  saturating to a plateau at large evolution times and momenta, obeying a power-law behavior with exponent  $\gamma = 2.8$ . The dashed line determines the threshold for quantifying  $|\mathbf{k}_{cf}|$ , see the discussion in the main text, and the vertical dash-dotted line marks  $|\mathbf{k}_{rot}|$ . The inset displays the ratio of integrated densities,  $n_x/n_y$ , signalling the isotropic dynamics for long evolution times. Panels (b) and (c) present the exponent dynamics  $\gamma(t)$  with respect to  $\omega_d$  in the case of a SS ( $a_i = 89 a_0$ ,  $a_f = 98 a_0$ ) and a SF ( $a_i = 98 a_0$ ,  $a_f = 91 a_0$ ) initial state respectively. Other parameters are the same as in Fig. 1.

fied by the power-law behavior of  $\tilde{n}(|\mathbf{k}|, t)$ . The time-evolution of the associated exponents for different driving frequencies is displayed in Fig. 2(c). It can be seen that they cluster around 3.26 (52) at  $t > 1000$  ms, namely at comparatively larger timescales required to observe the saturation of  $\gamma(t)$  in the opposite driving scenario [Fig. 2(b)]. This timescale prolongation is reminiscent of a shaken non-dipolar SF in a box [9], where the corresponding exponent converged towards 3.5 around 1.5 secs. Notice also that using a small driving amplitude  $a_f - a_i$ , where the dipolar gas remains within the same (SF or SS) phase, leads to weak density deformations without any evidence of wave turbulence, see also SM [51].

For completeness, we next explore the properties of the nonequilibrium quasi-steady state when transitioning from a SS to a dipolar droplet state [24]. In particular, we start from the same SS configuration as before with  $a_i = 89 a_0$ , see also Fig. 1(a), and deploy periodic modulation of the scattering length to  $a_f = 82 a_0$ . The latter gives rise to a localized array of isolated droplets in the quasi-2D ground state phase diagram [42]. However, in the course of the evolution a significant SF connection among the droplets persists, as shown in the in-

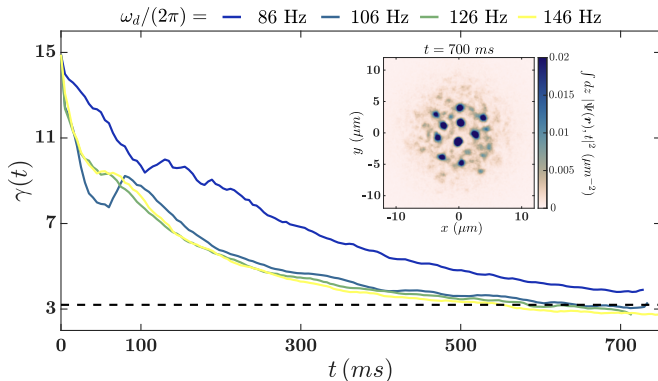


FIG. 3. Exponent dynamics at large momenta when dynamically crossing the SS ( $a_i = 89a_0$ ) to droplets ( $a_f = 82a_0$ ) phase boundary for different driving frequencies (see legend). A saturation of the exponent around 3.18 (dashed line) is observed evincing the approach to a quasi-steady state. The latter encompassing a SF background is visualized in the inset depicting the density profile  $\int dz |\Psi(\mathbf{r}, t)|^2$  across the plane pertaining to  $\omega_d = 2\pi \times 126$  Hz at long evolution times.

set of Fig. 3 referring to  $\omega_d = 2\pi \times 126$  Hz. This SF background along with the high-density peaks—similarly to what has been observed in the SF-to-SS transition and vice versa—becomes substantially perturbed at long timescales. Crucially, the exponents  $\gamma(t)$  obtained from the tails of  $\tilde{n}(|\mathbf{k}|, t)$  irrespectively of  $\omega_d$  [Fig. 3] attain the wave turbulence value  $\gamma(t \gtrsim 600 \text{ ms}) \approx 3.18$  (49), as indicated by the dashed line in Fig. 3. These are the same timescales as in the SS-to-SF transition [Fig. 2(b)]. Such an observation raises the question: why does the SS state facilitates the transition to wave turbulence faster than a SF?

*Cascade front dynamics.* The answer lies in the dynamics of the cascade front, which governs energy transport towards larger momenta in wave turbulence. The energy is carried by the cascade front  $|\mathbf{k}_{cf}|$ , associated with the cusp point where  $\tilde{n}(|\mathbf{k}|, t)$  falls faster than  $|\mathbf{k}|^{-\gamma}$  at large momenta [8]. As the cascade front propagates, it establishes the quasi-steady state in its wake. Within the framework of weak wave turbulence [7], the growth of the cascade front follows the scaling relation  $|\mathbf{k}_{cf}| \sim t^\beta$ , with exponent  $\beta = \frac{1}{2+d-\gamma}$  in  $d$ -dimensions. It is derived from energy and particle conservation laws and holds universally, i.e., regardless of the system microscopic characteristics, as long as the dispersion relation of elementary excitations is quadratic [13]. For a dipolar condensate, there is a linear phononic contribution at low momenta, followed by the roton minimum at intermediate momenta and afterwards the dispersion relation becomes quadratic [36]. The roton minimum for the SS initial state considered herein corresponds to  $|\mathbf{k}_{rot}|l_s \simeq 0.177$ ; see the vertical dash-dotted line in Fig. 2(a). Therefore, it is anticipated that the growth rate of energy to high momenta scales with the same exponent  $\beta$  for both SS

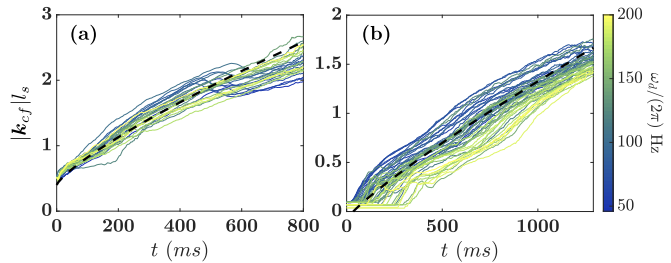


FIG. 4. Rescaled cascade front  $|\mathbf{k}_{cf}|l_s$  with respect to the driving frequency for the (a) SS [ $a_i (a_f) = 89 (98)a_0$ ], and (b) SF [ $a_i (a_f) = 98 (91)a_0$ ] initial states. The black dashed lines represent the fits  $|\mathbf{k}_{cf}| \sim t^\beta$ . The extended momentum distribution of the SS leads to a faster saturation of the cascade front compared to the SF initial state. Note that  $l_s = \hbar/\sqrt{m\mu}$  differs for the distinct initial states, since it depends on the chemical potential.

and SF initial states.

The cascade front is determined by the intersection of  $\tilde{n}(|\mathbf{k}|, t)(|\mathbf{k}|l_s)^\gamma$  and a threshold set at half of the nonequilibrium quasi-steady state plateau [13], see the horizontal dashed line in Fig. 2(a). Fitting  $|\mathbf{k}_{cf}|$  with  $t^\beta$  (dashed lines in Fig. 4), unveils the scaling exponent for the SS [Fig. 4(a)],  $\beta = 0.79(0.05)$ , which is indeed close to the one extracted for a dipolar SF [Fig. 4(b)], that is  $\beta = 0.8533(0.04)$ . The almost linear increase of the front,  $|\mathbf{k}_{cf}|$ , can be appreciated by setting  $d = 2$  and  $\gamma = 3$  in the scaling exponent  $\beta$ . Moreover, the scaling appears to be almost independent of  $\omega_d$ , which demonstrates once more the independence of the quasi-steady state on the driving.

Although the cascade front exhibits a similar growth in both dynamical crossings of the SS-to-SF transition, it starts from a larger value when the system resides in a SS phase, see Fig. 4(a). This difference arises because the momentum distribution of the latter possesses a larger amplitude at large  $|\mathbf{k}|$  compared to that of a SF, due to the high momentum peaks associated with the roton minimum [17]. Therefore, at a given time,  $|\mathbf{k}_{cf}|$  attains higher values in the case of a SS compared to a SF<sup>1</sup>.

Apart from  $|\mathbf{k}_{cf}|$ , the exponent  $\beta$  dictates the evolution of the momentum distribution prior to the establishment of the quasi-steady state. In particular, within weak wave turbulence the scaling relation  $\left(\frac{t}{t_0}\right)^{\gamma\beta} \tilde{n}(|\mathbf{k}|, t) = \tilde{n}(|\mathbf{k}|(t_0/t)^\beta, t_0)$  holds [13], where  $t_0$  is an arbitrary timescale. Exploiting this relation reveals that the curves of  $\tilde{n}(|\mathbf{k}|, t)(|\mathbf{k}|l_s)^\gamma$  at long time instants converge towards a narrow band regardless of the initial state unveiling the self-similar dynamics of the turbulent cascade.

<sup>1</sup> The long-time behavior of the cascade front depends on the chosen threshold. Namely, smaller thresholds lead to saturation of  $|\mathbf{k}_{cf}|$  at larger momenta. However, the scaling exponent  $\beta$  has a weak dependence on the threshold for both initial states.

*Conclusions.* We explicated the manifestation and properties of wave turbulence in driven dipolar gases featuring beyond mean-field corrections, while dynamically crossing the ensuing phase boundaries. The behavior of the spectrum at long timescales is unveiled associated with a direct energy cascade and the emergence of a genuine nonequilibrium quasi-steady state. The estimated scaling exponents at large momenta signal the onset of wave turbulence. Notably, we uncover that exotic phases of matter such as SS or droplets due to their inherent extended momentum distribution expedite the generation of the ensuing nonequilibrium quasi-steady state. We have demonstrated the emergence of wave turbulence independently of the initial phase, the driving frequency and the crossed phase boundary.

Our results open new avenues for the exploration of quantum turbulence and the universal features of nonequilibrium dynamics in long-range interacting platforms [17], even beyond dipolar gases, exhibiting, for instance, crystallized density order [3]. In this context, it would be valuable to explore how different exotic crystal arrangements [54, 55] (beyond the hexagonal one) can be systematically used to engineer the onset of turbulence. A natural next step is to investigate the emergence of the inverse energy cascade [11, 15, 56] in such long-range interacting setups with a particular focus on understanding the role of relevant beyond-mean-field phases of matter. Another interesting pathway is to explore non-conventional anisotropic turbulent aspects e.g. with the aid of a rotating magnetic field [57, 58].

*Acknowledgments.* S. I. M acknowledges support from the Missouri Science and Technology, Department of Physics, Startup fund. Financial support by the Knut and Alice Wallenberg Foundation and the Swedish Research Council are also acknowledged (K. M). S. I. M acknowledges extensive discussions with H. R. Sadeghpour in the context of universal dynamics and supersolid character. K.M gratefully acknowledges many discussions with Stephanie M. Reimann on the topic of supersolidity.

- 
- [1] A. N. Kolmogorov, Dokl. Akad. Nauk SSSR **30**, 301 (1941); A. Obukhov, in *Dokl. Akad. Nauk SSSR*, Vol. 32 (1941) p. 22; R. H. Kraichnan, *The Physics of Fluids* **10**, 1417 (1967); U. Frisch, *Turbulence: the legacy of AN Kolmogorov* (Cambridge university press, 1995).
- [2] P. A. Hwang, D. W. Wang, E. J. Walsh, W. B. Krabill, and R. N. Swift, *J. Phys. Oceanogr.* **30**, 2753 (2000); P. Cobelli, A. Prasadka, P. Petitjeans, G. Lagubeau, V. Pagneux, and A. Maurel, *Phys. Rev. Lett.* **107**, 214503 (2011).
- [3] H. J. Choi, S. T. Lim, P.-Y. Lai, and C. K. Chan, *Phys. Rev. Lett.* **89**, 088302 (2002).
- [4] N. A. Bakas and P. J. Ioannou, *Phys. Rev. Lett.* **110**, 224501 (2013); P. H. Diamond, S.-I. Itoh, K. Itoh, and T. S. Hahm, *Plasma Phys. Control. Fusion* **47**, R35 (2005).
- [5] P. Mösta, C. D. Ott, D. Radice, L. F. Roberts, E. Schnetter, and R. Haas, *Nature* **528**, 376 (2015).
- [6] A. J. Chorin, *Vorticity and Turbulence* (Springer, New York, 1994); J. Yao and F. Hussain, *Annu. Rev. Fluid Mech.* **54**, 317 (2022).
- [7] V. E. Zakharov, V. S. L’vov, and G. Falkovich, *Kolmogorov spectra of turbulence I: Wave turbulence* (Springer, 1992).
- [8] S. Nazarenko, *Wave turbulence*, Vol. 825 (Springer, 2011).
- [9] L. Madeira, M. A. Caracanhas, F. dos Santos, and V. S. Bagnato, *Annu. Rev. Condens. Matter Phys.* **11**, 37 (2020); M. C. Tsatsos, P. E. Tavares, A. Cidrim, A. R. Fritsch, M. A. Caracanhas, F. E. A. dos Santos, C. F. Barenghi, and V. S. Bagnato, *Phys. Rep.* **622**, 1 (2016); N. Navon, A. L. Gaunt, R. P. Smith, and Z. Hadzibabic, *Nature* **539**, 72 (2016); W. Vinen and J. Niemela, *J. Low Temp. Phys.* **128**, 167 (2002).
- [10] W. J. Kwon, G. Moon, J.-y. Choi, S. W. Seo, and Y.-i. Shin, *Phys. Rev. A* **90**, 063627 (2014).
- [11] E. A. L. Henn, J. A. Seman, G. Roati, K. M. F. Magalhães, and V. S. Bagnato, *Phys. Rev. Lett.* **103**, 045301 (2009); T. W. Neely, A. S. Bradley, E. C. Samson, S. J. Rooney, E. M. Wright, K. J. H. Law, R. Carretero-González, P. G. Kevrekidis, M. J. Davis, and B. P. Anderson, *Phys. Rev. Lett.* **111**, 235301 (2013); G. Gauthier, M. T. Reeves, X. Yu, A. S. Bradley, M. A. Baker, T. A. Bell, H. Rubinsztein-Dunlop, M. J. Davis, and T. W. Neely, *Science* **364**, 1264 (2019); S. P. Johnstone, A. J. Groszek, P. T. Starkey, C. J. Billington, T. P. Simula, and K. Helmerson, *Science* **364**, 1267 (2019); A. W. Baggaley and C. F. Barenghi, *Phys. Rev. B* **83**, 134509 (2011); M. E. Mossman, M. A. Hoefer, K. Julien, P. G. Kevrekidis, and P. Engels, *Nature Commun.* **9**, 4665 (2018).
- [12] M. Ghosh Dastidar, S. Das, K. Mukherjee, and S. Majumder, *Physics Letters A* **421**, 127776 (2022); S. Das, K. Mukherjee, and S. Majumder, *Phys. Rev. A* **106**, 023306 (2022); A. Bulgac, M. Kafker, I. Abdurrahman, and G. Wlazłowski, *Phys. Rev. Res.* **6**, L042003 (2024).
- [13] M. Gałka, P. Christodoulou, M. Gazo, A. Karailiev, N. Dogra, J. Schmitt, and Z. Hadzibabic, *Phys. Rev. Lett.* **129**, 190402 (2022); N. Navon, C. Eigen, J. Zhang, R. Lopes, A. L. Gaunt, K. Fujimoto, M. Tsubota, R. P. Smith, and Z. Hadzibabic, *Science* **366**, 382 (2019).
- [14] L. H. Dogra, G. Martirosyan, T. A. Hilker, J. A. Glidden, J. Etrych, A. Cao, C. Eigen, R. P. Smith, and Z. Hadzibabic, *Nature* **620**, 521 (2023); G. Martirosyan, K. Fujimoto, and N. Navon, arXiv:2407.08738 (2024); Y. Zhu, G. Krstulovic, and S. Nazarenko, arXiv:2408.15163 (2024).
- [15] A. Karailiev, M. Gazo, M. Gałka, C. Eigen, T. Satoor, and Z. Hadzibabic, arXiv preprint arXiv:2405.01537 (2024).
- [16] T. Bland, G. W. Stagg, L. Galantucci, A. Baggaley, and N. G. Parker, *Phys. Rev. Lett.* **121**, 174501 (2018).
- [17] L. Chomaz, I. Ferrier-Barbut, F. Ferlaino, B. Laburthe-Tolra, B. L. Lev, and T. Pfau, *Rep. Prog. Phys.* **86**, 026401 (2022); T. Lahaye, C. Menotti, L. Santos, M. Lewenstein, and T. Pfau,

- Rep. Prog. Phys. **72**, 126401 (2009).
- [18] S. Sabari, R. Kishor Kumar, and L. Tomio, Phys. Rev. A **109**, 023313 (2024).
- [19] S. B. Prasad, N. G. Parker, and A. W. Baggaley, “Crow instability of vortex lines in dipolar superfluids,” (2024), arXiv:2407.04177 [cond-mat.quant-gas].
- [20] S. Altmeyer, Y. Do, and Y.-C. Lai, Sci. Rep. **5**, 10781 (2015); S. Mouraya, N. Pan, and S. Banerjee, Phys. Rev. Fluids **9**, 094604 (2024); S. Altmeyer, Y. Do, and Y.-C. Lai, Sci. Rep. **5**, 18589 (2015).
- [21] M. Lu, N. Q. Burdick, S. H. Youn, and B. L. Lev, Phys. Rev. Lett. **107**, 190401 (2011).
- [22] K. Aikawa, A. Frisch, M. Mark, S. Baier, A. Rietzler, R. Grimm, and F. Ferlaino, Phys. Rev. Lett. **108**, 210401 (2012).
- [23] Y. Miyazawa, R. Inoue, H. Matsui, G. Nomura, and M. Kozuma, Phys. Rev. Lett. **129**, 223401 (2022).
- [24] H. Kadau, M. Schmitt, M. Wenzel, C. Wink, T. Maier, I. Ferrier-Barbut, and T. Pfau, Nature **530**, 194 (2016); M. Schmitt, M. Wenzel, F. Böttcher, I. Ferrier-Barbut, and T. Pfau, Nature **539**, 259 (2016); I. Ferrier-Barbut, H. Kadau, M. Schmitt, M. Wenzel, and T. Pfau, Phys. Rev. Lett. **116**, 215301 (2016); L. Chomaz, S. Baier, D. Petter, M. J. Mark, F. Wächtler, L. Santos, and F. Ferlaino, Phys. Rev. X **6**, 041039 (2016).
- [25] F. Wächtler and L. Santos, Phys. Rev. A **94**, 043618 (2016).
- [26] F. Wächtler and L. Santos, Phys. Rev. A **93**, 061603 (2016).
- [27] G. V. Chester, Phys. Rev. A **2**, 256 (1970).
- [28] A. J. Leggett, Phys. Rev. Lett. **25**, 1543 (1970).
- [29] L. Tanzi, S. M. Rocuzzo, E. Lucioni, F. Fama, A. Fioretti, C. Gabbanini, G. Modugno, A. Recati, and S. Stringari, Nature **574**, 382–385 (2019).
- [30] F. Böttcher, J.-N. Schmidt, M. Wenzel, J. Hertkorn, M. Guo, T. Langen, and T. Pfau, Phys. Rev. X **9**, 011051 (2019).
- [31] L. Chomaz, D. Petter, P. Ilzhöfer, G. Natale, A. Trautmann, C. Politi, G. Durastante, R. M. W. van Bijnen, A. Patscheider, M. Sohmen, M. J. Mark, and F. Ferlaino, Phys. Rev. X **9**, 021012 (2019).
- [32] L. Tanzi, S. M. Rocuzzo, E. Lucioni, F. Fama, A. Fioretti, C. Gabbanini, G. Modugno, A. Recati, and S. Stringari, Nature **574**, 382–385 (2019).
- [33] M. A. Norcia, C. Politi, L. Klaus, E. Poli, M. Sohmen, M. J. Mark, R. N. Bisset, L. Santos, and F. Ferlaino, Nature **596**, 357 (2021).
- [34] G. Biagioni, N. Antolini, A. Alaña, M. Modugno, A. Fioretti, C. Gabbanini, L. Tanzi, and G. Modugno, Phys. Rev. X **12**, 021019 (2022).
- [35] T. Bland, E. Poli, C. Politi, L. Klaus, M. A. Norcia, F. Ferlaino, L. Santos, and R. N. Bisset, Phys. Rev. Lett. **128**, 195302 (2022).
- [36] D. Petter, G. Natale, R. van Bijnen, A. Patscheider, M. Mark, L. Chomaz, and F. Ferlaino, Phys. Rev. Lett. **122**, 183401 (2019).
- [37] M. Guo, F. Böttcher, J. Hertkorn, J.-N. Schmidt, M. Wenzel, H. P. Büchler, T. Langen, and T. Pfau, Nature **574**, 386–389 (2019).
- [38] M. Boninsegni and N. V. Prokof’ev, Rev. Mod. Phys. **84**, 759 (2012).
- [39] E. Poli, D. Baillie, F. Ferlaino, and P. B. Blakie, “Excitations of a two-dimensional supersolid,” (2024), arXiv:2407.01072 [cond-mat.quant-gas].
- [40] T. D. Lee, K. Huang, and C. N. Yang, Phys. Rev. **106**, 1135 (1957).
- [41] A. R. P. Lima and A. Pelster, Phys. Rev. A **84**, 041604 (2011).
- [42] D. Baillie and P. B. Blakie, Phys. Rev. Lett. **121**, 195301 (2018).
- [43] E. Casotti, E. Poli, L. Klaus, A. Litvinov, C. Ulm, C. Politi, M. J. Mark, T. Bland, and F. Ferlaino, “Observation of vortices in a dipolar supersolid,” (2024), arXiv:2403.18510 [cond-mat, physics.quant-ph] version: 1.
- [44] T. Bland, E. Poli, C. Politi, L. Klaus, M. Norcia, F. Ferlaino, L. Santos, and R. Bisset, Phys. Rev. Lett. **128**, 195302 (2022).
- [45] S. Ronen, D. C. E. Bortolotti, D. Blume, and J. L. Bohn, Phys. Rev. A **74**, 033611 (2006).
- [46] S. Yi and L. You, Phys. Rev. A **63**, 053607 (2001).
- [47] C. Chin, R. Grimm, P. Julienne, and E. Tiesinga, Rev. Mod. Phys. **82**, 1225 (2010).
- [48] T. Maier, I. Ferrier-Barbut, H. Kadau, M. Schmitt, M. Wenzel, C. Wink, T. Pfau, K. Jachymski, and P. S. Julienne, Phys. Rev. A **92**, 060702 (2015).
- [49] A. R. P. Lima and A. Pelster, Phys. Rev. A **84**, 041604 (2011).
- [50] R. Schützhold, M. Uhlmann, Y. Xu, and U. R. Fischer, Int. J. Mod. Phys. B **20**, 3555 (2006).
- [51] In the Supplementary Material [URL] more information can be found regarding the inclusion of three-body losses and dissipation, the absence of turbulence for small driving amplitudes, and details on our simulations.
- [52] Y. Zhu, B. Semisalov, G. Krstulovic, and S. Nazarenko, Phys. Rev. Lett. **130**, 133001 (2023).
- [53] G. V. Kolmakov, P. V. E. McClintock, and S. V. Nazarenko, PNAS **111**, 4727 (2014).
- [54] B. T. E. Ripley, D. Baillie, and P. B. Blakie, Phys. Rev. A **108**, 053321 (2023).
- [55] J. Hertkorn, J.-N. Schmidt, M. Guo, F. Böttcher, K. S. H. Ng, S. D. Graham, P. Uerlings, T. Langen, M. Zwierlein, and T. Pfau, Phys. Rev. Res. **3**, 033125 (2021).
- [56] M. T. Reeves, T. P. Billam, B. P. Anderson, and A. S. Bradley, Phys. Rev. Lett. **110**, 104501 (2013).
- [57] S. Halder, K. Mukherjee, S. I. Mistakidis, S. Das, P. G. Kevrekidis, P. K. Panigrahi, S. Majumder, and H. R. Sadeghpour, Phys. Rev. Res. **4**, 043124 (2022).
- [58] K. Mukherjee, M. N. Tengstrand, T. A. Cardinale, and S. M. Reimann, Phys. Rev. A **108**, 023302 (2023).

# Supplementary Material: Wave turbulence in driven dipolar gases

## TURBULENCE IN THE PRESENCE OF THREE-BODY LOSSES

It is known that the many-body self-bound SS and droplet states suffer from three-body recombination processes experimentally [S1] since they exhibit high densities. A question that arises is whether the relevant three-body loss mechanisms might impede the experimental detection of wave turbulence, given that it occurs over long evolution times. To facilitate corresponding experimental endeavors, here, we demonstrate that the inclusion of three-body losses does not prevent the emergence of wave turbulence. We substantiate this argument by using the SS as an initial state with  $a_i = 89 a_0$ , and subsequently dynamically cross the SF boundary upon considering  $a_f = 98 a_0$  and a driving frequency  $\omega_d = 2\pi \times 127$  Hz. To take into account three-body losses, we assume the additional imaginary term  $-i\hbar \frac{L_3}{2} |\Psi|^4 \Psi$  to the right hand side of the extended Gross-Pitaevskii equation [Eq. (1) in the main text] used to monitor the nonequilibrium dynamics of the dipolar gas under periodic driving. Here,  $L_3$  denotes the three-body recombination rate, which for  $^{164}\text{Dy}$  is taken to be  $L_3 = 1.2 \times 10^{-41} m^6/s$  [S2] according to Ref. [S3].

Despite the occurrence of three-body losses, the dipolar SS still clearly enters the wave turbulent regime at long evolution times, as evidenced by the power law behavior at large momenta shown in the inset of Fig. S1(a), with  $\gamma = 3.09$ . In particular, a plateau appears in the compensated spectrum [Fig. S1(a)] around  $|\mathbf{k}|l_s \simeq 1$  at  $t > 600$  ms, signalling the emergence of a nonequilibrium quasi-steady state. A similar behavior of the compensated spectrum occurs also for other driving frequencies (not shown for brevity). The fitted exponent [solid line in Fig. S1(b)] lies very close to the one pertaining to  $L_3 = 0$  (dashed line) during the dynamics, displaying negligible deviations at late evolution times. Both of the exponents eventually saturate in the ballpark of 3, which is the value predicted from weak wave turbulence [S4]. For completeness, we remark that within the presented timescales the particle number drops to around  $\simeq 70\%$  of the initial atom number  $N_0 = 8 \times 10^4$ , see the inset of Fig. S1(b). This is also manifested by the smaller amplitude of the compensated momentum distribution [Fig. S1(a)] in comparison to the respective one without three-body losses [Fig. 2(a) in the main text]. This behavior is particularly pronounced at large momenta, where  $\tilde{n}(|\mathbf{k}|, t)(|\mathbf{k}|l_s)^\gamma$  [Fig. S1(a)] displays a much steeper descend than without the  $L_3$  coefficient. Moreover, the SS nature of the dynamical state is still preserved within the timescales that the quasi-steady state is reached.

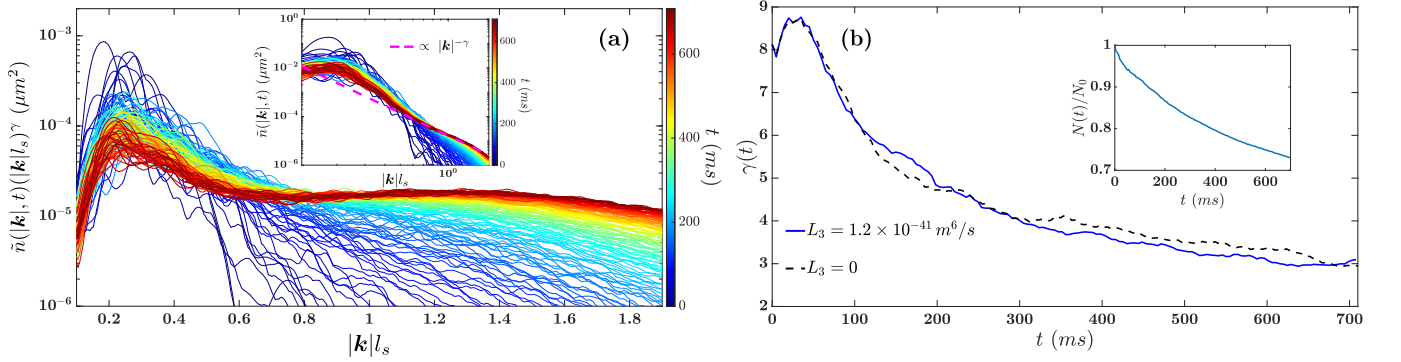


FIG. S1. Emergence of wave turbulence in a driven SS in the presence of three-body recombination. (a) Compensated spectrum with the inclusion of three-body losses for  $a_i = 89 a_0$ ,  $a_f = 98 a_0$  and  $\omega_d = 2\pi \times 127$  Hz as in Fig. 2(a) of the main text. Saturation of the spectrum at  $t > 500$  ms takes place manifesting the approach to turbulent behavior. The inset presents the  $|\mathbf{k}|^{-\gamma}$  power-law fitting of the momentum distribution in the range  $|\mathbf{k}|l_s \simeq 1$ . (b) Comparison between the exponent dynamics at large momenta with finite and zero three-body recombination (see legend). As it can be seen, there are no appreciable deviations imprinted in the exponent between the finite  $L_3$  and  $L_3 = 0$  scenario, while in both cases the exponent saturates close to  $\approx 3.09$ . The inset presents the particle number during the time evolution, normalized to the initial number  $N_0 = 8 \times 10^4$ . Even for the  $\sim 30\%$  atom losses occurring at long evolution times a SS structure persists.

## ABSENCE OF TURBULENCE FOR DRIVING WITHIN THE SAME PHASE

In the main text, it is argued that, regardless of the initial state (SF, SS, or droplet), when the dipolar gas is periodically driven across one of the resulting phase transitions, it exhibits wave turbulence in the later stages of the evolution. Here, we demonstrate that employing sufficiently small driving amplitudes,  $a_f - a_i$ , which ensure that the

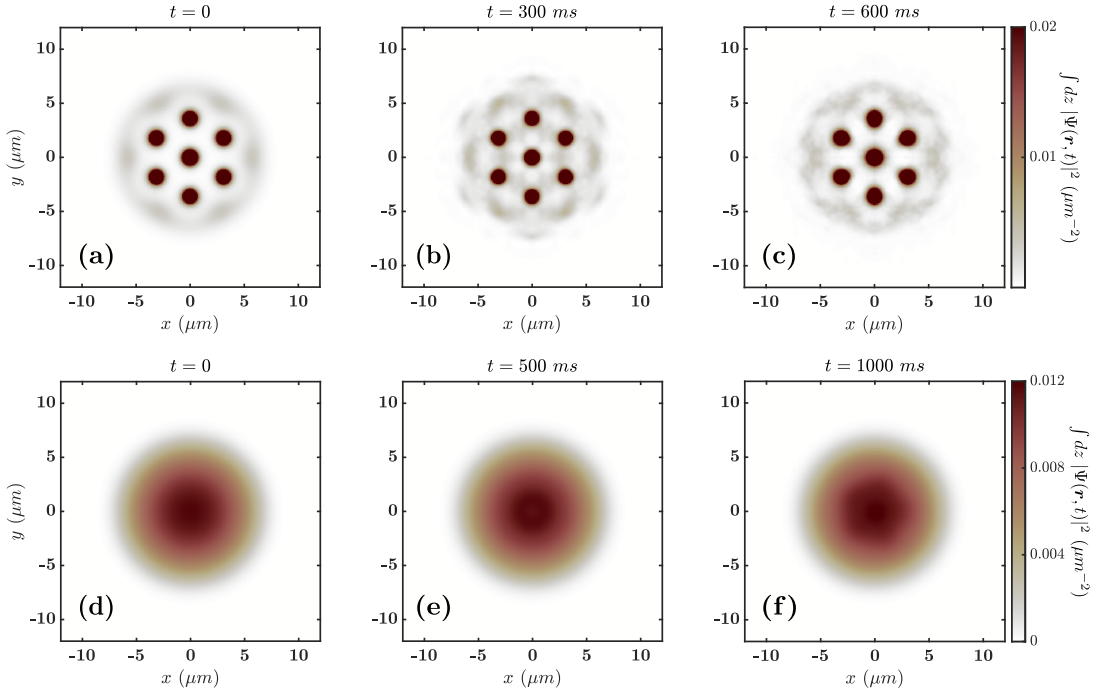


FIG. S2. Absence of wave turbulence for a dipolar gas driven within the same phase. Density snapshots (integrated along the transverse direction) across the  $x$ - $y$  plane for an initial (a)-(c) SS with  $a_i = 89 a_0$  and (d)-(f) a SF at  $a_i = 98 a_0$ . Evidently, the SS features a distorted background while the SF performs a collective motion. The driving amplitude,  $|a_f - a_i| = 2 a_0$ , is relatively small in both cases such that the underlying ground state phase boundary is not dynamically crossed. The used driving frequencies are  $\omega_d = 2\pi \times 127$  Hz and  $\omega_d = 2\pi \times 85$  Hz for the SS and SF respectively.

dipolar gas remains in the same phase dynamically, prevents the manifestation of a turbulent response, irrespective of the initial state. To substantiate our argument we present the nonequilibrium dynamics when the dipolar BEC is initiated either in the SF or the SS state and it is subsequently under the influence of a sinusoidally modulated 3D scattering length with an amplitude that does not exceed any relevant phase boundary. The density snapshots of the driven dipolar gas are presented in Fig. S2. Starting from a SS state characterized by  $a_i = 89 a_0$  we observe that, upon driving with  $a_f = 91 a_0$  and  $\omega_d = 2\pi \times 127$  Hz, only relatively small amplitude density undulations develop on top of the original hexagonal structure distorting the background SF but not the droplet arrangement, see the integrated density profiles depicted in Fig. S2(a)-(c). This response remains the same for longer timescales and holds for different driving frequencies that we have checked. Turning to a driven dipolar SF with  $a_i = 98 a_0$ ,  $a_f = 96 a_0$  and  $\omega_d = 2\pi \times 85$  Hz, illustrated in Fig. S2(d)-(f), it can be seen that collective motion of the background occurs in the form of an isotropic breathing mode. This is accompanied by signatures of developing bulk structures such as the hexagonal pattern appearing in Fig. S2(f). The spontaneous generation of such patterns is another interesting venue for future research in terms of exploiting parametric instabilities [S5, S6].

## TURBULENCE IN THE PRESENCE OF DISSIPATION

As demonstrated in the main text, energy is transported to smaller length scales by means of nonlinear wave interference resulting in wave turbulence. Additionally, we have considered a fully condensed gas without any damping channels. In the following, we study the emergent non-equilibrium dynamics by including a phenomenological damping term,  $\kappa$ , to the extended Gross-Pitaevskii equation [S7–S10],

$$(i - \kappa)\hbar\partial_t\Psi(\mathbf{r}, t) = \left[ -\frac{\hbar^2}{2m}\nabla^2 + V(\mathbf{r}) + \frac{4\pi\hbar^2 a}{m}|\Psi(\mathbf{r}, t)|^2 + \int d\mathbf{r}' U_{dd}(\mathbf{r} - \mathbf{r}')|\Psi(\mathbf{r}', t)|^2 + \gamma(\epsilon_{dd})|\Psi(\mathbf{r}, t)|^3 \right] \Psi(\mathbf{r}, t). \quad (\text{S1})$$

The significance of  $\kappa$  becomes apparent when the above equation is expressed in the hydrodynamical formalism, where  $\hbar\kappa/(2m)$  plays the role of viscosity, dubbed the kinematic quantum viscosity [S11]. In that regard, the damping factor

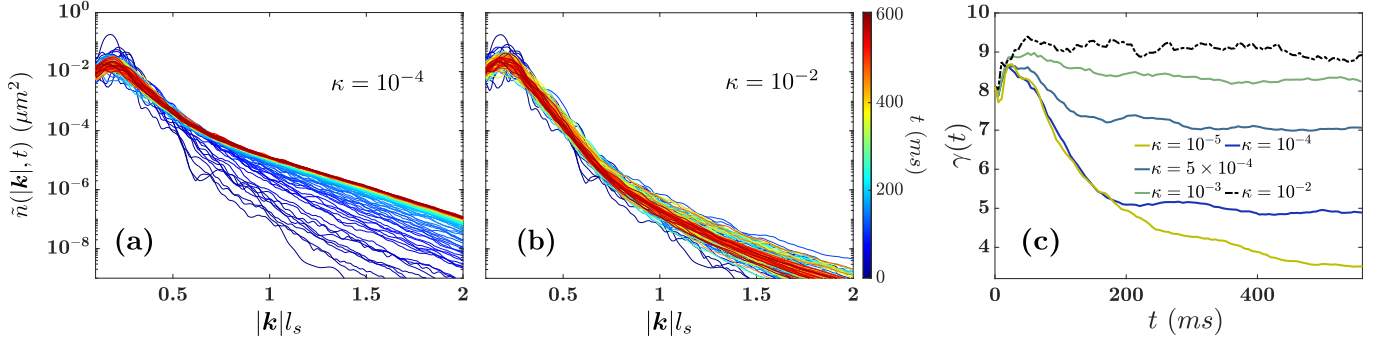


FIG. S3. Emergence of quasi-steady state at long evolution times in the presence of dissipation. Dynamics of the momentum distributions of an initial SS ( $a_i = 89 a_0$ ) undergoing through the SS-to-SF transition with  $a_f = 98 a_0$ ,  $\omega_d = 2\pi \times 127$  Hz and phenomenological damping (a)  $\kappa = 10^{-4}$  and (b)  $\kappa = 10^{-2}$  respectively. (c) Time evolution of the exponents at large momenta for different phenomenological damping terms (see legend). A large  $\kappa$  facilitates the suppression of the large momentum tails, and hence it leads to significantly elevated exponents at late time instants.

$\kappa$  usually depends on temperature, and is inversely proportional to the relaxation time of the dipolar BEC [S12].

To develop an understanding on how dissipation affects the onset of turbulence for the SS-to-SF dynamical crossing, we consider  $\kappa$  in the range  $[10^{-5}, 10^{-2}]$ . The influence of damping can be readily seen by contrasting the momentum distributions in Fig. S3(a),(b). A larger  $\kappa$  leads to the decay of high momentum excitations of the system that would otherwise be responsible for carrying energy to small length scales in the direct turbulent cascade. Instead, the high momentum tail of  $\tilde{n}(|\mathbf{k}|, t)$  is highly suppressed, and even at large evolution times, the distribution remains close to the initial one. Such an equilibration process is observed also in the time evolution of the extracted exponent at large momenta [Fig. S3(c)]. For  $\kappa = 10^{-5}$ , which represents adequately small dissipation, the exponent quickly decreases and saturates close to the value obtained in the absence of dissipation (i.e.  $\gamma = 3.5$ ). For a larger  $\kappa = 10^{-4}$ ,  $\gamma(t)$  still saturates, but to a plateau whose value is larger than what is anticipated for weak wave turbulence. As the damping term increases further,  $\gamma(t)$  fluctuates close to its initial value.

### SIMULATION DETAILS

To numerically tackle the ground state properties and the nonequilibrium dynamics of the considered quasi-2D dipolar gas we simulate the extended Gross-Pitaevskii equation (1) provided in the main text. For numerical convenience it is casted in a dimensionless form. Specifically, space and time scales are expressed in units of the harmonic oscillator length  $a_{ho} = \sqrt{\hbar/(m\omega_x)}$  and  $\omega_x^{-1}$  respectively. Moreover, the 3D wave function is rescaled according to  $\Psi(\mathbf{r}, t) = \sqrt{N/a_{ho}^3} \Psi'(\mathbf{r}', t')$ , where the prime quantities refer to dimensionless ones. Note that this rescaling implies that the  $\Psi'$  wave function is normalized to unity, i.e.  $\int d\mathbf{r}' |\Psi'(\mathbf{r}', t')|^2 = 1$ . Additionally, the three-dimensional space is discretized in a uniform cubic grid of  $512 \times 512 \times 128$  points along the  $x$ ,  $y$  and  $z$  directions respectively with spatial discretization  $\delta x = \delta y = 0.08 a_{ho}$  in the plane and  $\delta z = 0.2 a_{ho}$  in the transverse direction. The time step of the numerical integrator is set to  $\delta t = 10^{-4}/\omega_x$  for both the imaginary and real time propagation of Eq. (1) in the main text. These are carried out by means of the split-step Crank-Nicolson numerical scheme [S13, S14]. In order to deal with the divergent behavior of the integrand present in the dipolar interaction integral [Eq. (1) in the main text], we utilize the convolution theorem [S15, S16]. In this way, the interaction integral is expressed as the inverse Fourier transform of the product of Fourier transforms of the dipolar interaction and wave function respectively.

To numerically obtain the exotic ground states of the dipolar gas, namely the SF, SS and droplet phases, the following initial ansatz is utilized

$$\Psi'(x', y', z', t = 0) = \mathcal{A} \left[ \cos\left(\frac{2\pi x'}{3}\right) + \cos\left(\frac{\pi x'}{3} + \frac{\pi y'}{\sqrt{3}}\right) + \cos\left(-\frac{\pi x'}{3} + \frac{\pi y'}{\sqrt{3}}\right) \right]^4 e^{-0.01[(x')^2 + (y')^2] - (\omega_z/\omega_x)(z')^2/2}, \quad (\text{S2})$$

with  $\mathcal{A}$  being a normalization constant. This ansatz is particularly tailored for capturing the six-fold symmetry of the cylindrically symmetric SS configurations [S17]. During every step of the imaginary time propagation, the dimensionless wave function is rescaled,  $\Psi' \rightarrow \Psi'/\|\Psi'\|$ , where  $\|\Psi'\| \equiv \int d\mathbf{r}' |\Psi'|^2$  denotes the norm, ensuring that the normalization is preserved. The ground state is identified by requiring that the relative difference between the wave

functions in two consecutive time steps of the imaginary time propagation is lower than  $10^{-4}$  and the corresponding energy deviations do not exceed  $10^{-8}$ . This state is subsequently employed for the real time dynamics of Eq. (1) in the main text. Our spatial and time ( $\delta t$ ) discretizations are chosen such that  $(\delta t)^2 < \delta x \delta y$  holds and as a consequence the real time dynamics is accurately simulated. Namely, the total particle number and energy are numerically conserved within the order of  $10^{-6}$  in the course of the evolution.

- 
- [S1] F. Böttcher, J.-N. Schmidt, M. Wenzel, J. Hertkorn, M. Guo, T. Langen, and T. Pfau, *Phys. Rev. X* **9**, 011051 (2019).  
[S2] F. Wächtler and L. Santos, *Phys. Rev. A* **93**, 061603 (2016).  
[S3] E. Casotti, E. Poli, L. Klaus, A. Litvinov, C. Ulm, C. Politi, M. J. Mark, T. Bland, and F. Ferlaino, arXiv:2403.18510 (2024).  
[S4] S. Nazarenko, *Wave turbulence*, Vol. 825 (Springer, 2011).  
[S5] K. Kwon, K. Mukherjee, S. J. Huh, K. Kim, S. I. Mistakidis, D. K. Maity, P. G. Kevrekidis, S. Majumder, P. Schmelcher, and J.-y. Choi, *Phys. Rev. Lett.* **127**, 113001 (2021).  
[S6] N. Liebster, M. Sparn, E. Kath, K. Fujii, S. Görlitz, T. Enss, H. Strobel, and M. K. Oberthaler, arXiv e-prints, arXiv (2023).  
[S7] S. Choi, S. A. Morgan, and K. Burnett, *Phys. Rev. A* **57**, 4057 (1998).  
[S8] L. Pitaevskii, *Sov. Phys.—JETP* **8**, 282 (1959).  
[S9] T. Bland, E. Poli, C. Politi, L. Klaus, M. Norcia, F. Ferlaino, L. Santos, and R. Bisset, *Phys. Rev. Lett.* **128**, 195302 (2022).  
[S10] E. B. Linscott and P. B. Blakie, *Phys. Rev. A* **90**, 053605 (2014).  
[S11] A. S. Bradley and B. P. Anderson, *Phys. Rev. X* **2**, 041001 (2012).  
[S12] N. P. Proukakis, G. Rigopoulos, and A. Soto, arXiv:2407.20178 (2024).  
[S13] J. Crank and P. Nicolson, in *Math. Proc. Camb. Philos. Soc.*, Vol. 43 (Cambridge University Press, 1947) pp. 50–67.  
[S14] X. Antoine, W. Bao, and C. Besse, *Comput. Phys. Commun.* **184**, 2621 (2013).  
[S15] G. B. Arfken and H.-J. Weber, *Mathematical methods for physicists* (Academic Press Orlando, FL, 1972).  
[S16] K. Góral and L. Santos, *Phys. Rev. A* **66**, 023613 (2002).  
[S17] D. Baillie and P. B. Blakie, *Phys. Rev. Lett.* **121**, 195301 (2018).